Surface-Wave Minimization Using Spherical Wave Expansion

Albert Salmi, Anu Lehtovuori, and Ville Viikari, *Senior Member, IEEE*

***Abstract*—This letter presents a method for reducing antenna-excited surface waves in mobile devices. Surface waves are canceled either by actively injecting compensating surface waves in opposite phase, or passively creating reactive conditions from which scattered, secondary surface waves cancel the primary waves. We use spherical wave expansion to calculate the amplitudes and phases of the canceling surface waves and show also how reactive loading near the antenna can launch these canceling waves. We verify the proposed method with simulations. Reduced surface waves result in a smoother radiation pattern and significantly increased gain.**

***Index Terms*—Millimeter-wave (mm-wave) antennas, mobile devices, spherical wave expansion, surface waves.**

I. Introduction

ANTENNA design for mobile devices at sub-6 GHz frequencies and millimeter-waves (mm-waves) differ in a fundamental manner. Low-frequency antennas are merely coupling elements rather than antennas, because they excite a surface current distribution on the chassis of the device [1]. The excited current distribution on the chassis may contribute more to radiation than currents in the actual antenna element [2]. This mechanism can be considered as an intentional excitation of standing waves on the surface of the device.

The situation is very different at mm-wave frequencies, where the device is electrically large. In such a case, surface waves cause many undesired effects. At these frequencies, small physical details of the device are significant for propagating surface waves, and discontinuities, such as an edge of the display, cause radiation. Together with the original radiator, the discontinuities form a sparse and irregular antenna array whose radiation pattern is ripply and gain possibly low. Moreover, the surface waves propagate in lossy materials, such as in the display of a mobile phone, which may result in the decrease of radiation efficiency.

Electromagnetic bandgap (EBG) structures [3]–[5] have been used to minimize surface waves, but often they require space that is not available in mobile devices. In some cases, the antenna itself can be designed to avoid excitation of surface waves [6], [7]. However, these methods are difficult to apply to structures other than microstrip antennas. Integrating an optically transparent metal mesh in a display [8] is an interesting idea, but its implementation in practical devices might be expensive and the solution might interfere with optically transparent electrodes used in capacitive touch screens.

Manuscript received 21 April 2022; accepted 12 May 2022. Date of publication 20 May 2022; date of current version 4 August 2022. *(Corresponding author: Albert Salmi.)*

The authors are with the Department of Electronics and Nanoengineering, Aalto University, 02150 Espoo, Finland (e-mail: albert.salmi@aalto.fi; anu.lehtovuori@aalto.fi; ville.viikari@aalto.fi).

Digital Object Identifier 10.1109/LAWP.2022.3176096

We propose a surface-wave minimization method that requires only small modifications close to the antenna, and thus, only minor modifications to the wireless device are needed. The surface waves are minimized based on far-field data only, so the method does not require in-depth analysis of the surface waves. The far fields are analyzed through the spherical wave expansion (SWE), which was earlier applied to antenna measurements, especially in near-field to far-field transformations [9]. In addition, the SWE has been utilized in antenna-radiation beam synthesis [10], [11]. Now, we use the SWE to characterize effects of the surface waves efficiently.

The idea of the proposed method is to launch additional surface waves in suitable amplitude and phase onto the device so that they cancel out the surface waves generated by the antenna. The canceling surface waves can be injected actively or created passively with properly loaded scatterers on the surface. The SWE is utilized to compute the canceling wave amplitudes and phases. We verify the method using simulations of a structure that models the display of a mobile phone. The method is demonstrated using both actively injected waves as well as passive scatterers.

II. Method for Surface-Wave Cancellation

A. Surface-Wave Analysis Through Spherical Harmonics

Fig. 1 illustrates the idea behind the proposed method. The sphere Ω_{A} encloses the antenna that generates the main radiation beam. The sphere Ω_{D} encloses the full device, including the region where both the antenna and the surface waves in the device contribute to the radiation. As a consequence of the surface waves, the field radiated from Ω_{D} has a ripply angular spread compared to the field radiated from Ω_{A}, as shown in the figure.

The degree of a spherical harmonic mode j is related to the number of zeros in θ-dependence of the mode's radiation pattern which implies that a ripply field must contain high degree modes. Also, the maximum degree of radiating modes correlates with the size of the radiating structure [12]. Thus, we know that only the lowest degree spherical harmonic modes contribute to the field radiated from Ω_{A}, whereas the field radiated from Ω_{D} may also contain high-degree modes. In addition, we know that the surface waves propagate mainly outside of Ω_{A}. This gives the basis of the method. By canceling out the high-degree spherical-harmonic modes, we can eliminate the effect of the surface waves on the radiation.

In this letter, we generate additional waves onto the surface of the device using additional excitations, so called control ports, which are placed close to the antenna. By choosing the amplitudes and phases appropriately based on the SWE, the high-degree spherical harmonic modes cancel each other out.

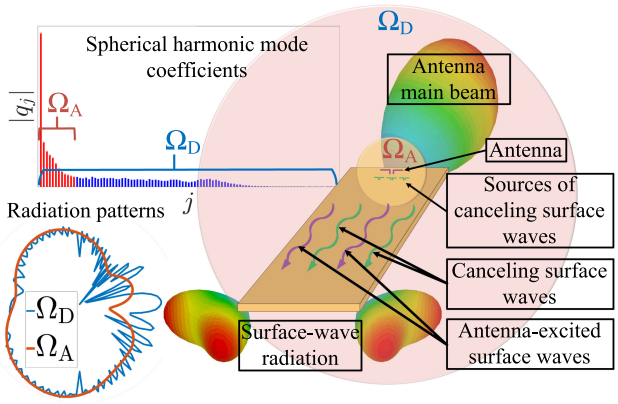

Fig. 1. Illustration of the idea of the proposed method.

Consequently, the surface waves are suppressed. The canceling can also be implemented passively. By terminating the control ports in suitable impedance loads, the scattered waves contain the same spherical harmonic modes as the waves excited by the active control ports.

B. Spherical Wave Expansion

An electric far field $\vec{E}(r,\theta,\varphi)$ can be expressed as a weighted sum of spherical waves $\vec{K}_{\text{smn}}(\theta,\varphi)$ defined in [12], as

$$\vec{E}(r,\theta,\varphi) = \frac{\sqrt{\eta}ke^{-ikr}}{\sqrt{4\pi}kr}\sum_{s=1}^{2}\sum_{n=1}^{N}\sum_{m=-n}^{n} q_{\text{smn}}\vec{K}_{\text{smn}}(\theta,\varphi) \quad (1)$$

where η is the wave impedance, k the wave number, and q_{smn} is the complex-valued expansion coefficient of the spherical harmonic mode of degree n and order m. The far-field spherical waves $\vec{K}_{\text{smn}}(\theta,\varphi)$ are power-normalized dimensionless solutions to vector wave equation. The time dependence is chosen to be $e^{i\omega t}$ in this letter.

In order to simplify the notation, we express the spherical wave expansion as

$$\vec{E}(\theta,\varphi) = \sum_{j=1}^{J} q_j\vec{K}_j(\theta,\varphi) \quad (2)$$

where $j = 2(n(n+1)+m-1)+s$ is a spherical harmonic-mode index and $J = 2N(N+2)$ is the maximum number of modes [12]. In this notation, the factors before the sum in (1) are included in the coefficients q.

The expansion coefficients can be determined by forming a linear system of equations from (2), and solving it, as done, for example, in [13]. Nevertheless, since the spherical waves are orthogonal and normalized with respect of radiated power, we can calculate the q-coefficients as

$$q_j = \frac{1}{4\pi}\int_0^{2\pi}\int_0^{\pi}\vec{E}(r,\theta,\varphi)\cdot\vec{K}_j^*(\theta,\varphi)\,\sin\theta\,\mathrm{d}\theta\mathrm{d}\varphi \quad (3)$$

where * is complex conjugation and the radius of the measurement sphere r is constant.

C. Excitation Weights of the Canceling Surface Waves

Next, we formulate an algorithm to calculate the amplitudes and phases of the canceling surface waves. These are the complex feeding signals in additional control ports if the canceling waves are excited actively.

The total number of ports in the antenna is P. The indices $p \in [1, p']$ refer to the antenna feeding ports and $p \in [p'+1, P]$ to the control ports. Each port radiates an electric far field $\vec{E}^p$. The total electric field radiated by the antenna and by the control ports is in terms of spherical waves

$$\vec{E} = \sum_{p=1}^{P} a_p\vec{E}^p = \sum_{p=1}^{P} a_p\sum_{j=1}^{J} q_j^p\vec{K}_j \quad (4)$$

where the complex coefficients a_p are the feeding signals of the ports.

Using matrix presentation, the field can be expressed as

$$\boldsymbol{E} = \mathbf{K}\mathbf{Q}\boldsymbol{a} \quad (5)$$

where $\boldsymbol{a} = [a_1,\ldots,a_P]^T \in \mathbb{C}^{P\times 1}$. The elements of $\mathbf{Q} \in \mathbb{C}^{J\times P}$ are $\mathbf{Q}_{jp} = q_j^p$. The electric-field vector and the matrix of the spherical waves are

$$\boldsymbol{E} = \begin{bmatrix}\boldsymbol{E}^\theta\\ \boldsymbol{E}^\varphi\end{bmatrix} \in \mathbb{C}^{2L\times 1} \quad \text{and} \quad \mathbf{K} = \begin{bmatrix}\mathbf{K}^\theta\\ \mathbf{K}^\varphi\end{bmatrix} \in \mathbb{C}^{2L\times J} \quad (6)$$

respectively. The elements of $\boldsymbol{E}^\theta$ and $\boldsymbol{E}^\varphi$ are of the form $\boldsymbol{E}_l^\alpha = \vec{E}(\theta_l,\varphi_l)\cdot\vec{u}_\alpha$, and $\vec{u}_\alpha$ is an α-oriented unit vector. The elements of $\mathbf{K}^\theta$ and $\mathbf{K}^\varphi$ are $\mathbf{K}_{lj}^\alpha = \vec{K}_j(\theta_l,\varphi_l)\cdot\vec{u}_\alpha$. The subscript $l \in [1,L] \subset \mathbb{N}$ refers to an observation point on the sphere, and j refers to the spherical harmonic mode.

Dividing the expansion coefficient matrix into four blocks gives

$$\mathbf{Q} = \begin{bmatrix}\breve{\mathbf{Q}}^{\text{A}} & \breve{\mathbf{Q}}^{\text{C}}\\ \hat{\mathbf{Q}}^{\text{A}} & \hat{\mathbf{Q}}^{\text{C}}\end{bmatrix}. \quad (7)$$

The submatrices $\breve{\mathbf{Q}}^{\text{A}}$ and $\breve{\mathbf{Q}}^{\text{C}}$ are the expansion coefficients of low-degree modes ($j < j'$) of the antenna feeding ports and control ports, respectively. We denote $j' \in [0, J] \subset \mathbb{N}$ as a limit between low and high degree modes. Similarly, $\hat{\mathbf{Q}}^{\text{A}}$ and $\hat{\mathbf{Q}}^{\text{C}}$ are the expansion coefficients of high-degree modes ($j \geqslant j'$). Correspondingly, the feeding-weight vector is divided into two blocks representing the feeding weights of the antenna ports and the control ports separately as

$$\boldsymbol{a} = \begin{bmatrix}\boldsymbol{a}^{\text{A}}\\ \boldsymbol{a}^{\text{C}}\end{bmatrix}. \quad (8)$$

Since we assume that the high-degree modes are consequence of surface waves, our target field is $\boldsymbol{E}^{\text{G}} = \mathbf{K}\boldsymbol{q}^{\text{G}}$, where

$$\boldsymbol{q}^{\text{G}} = \begin{bmatrix}\breve{\boldsymbol{q}}^{\text{G}}\\ \mathbf{0}\end{bmatrix}. \quad (9)$$

The target field represented by the vector $\boldsymbol{q}^{\text{G}}$ does not include high-degree modes. The goal is to find feeding weights for control ports $\boldsymbol{a}^{\text{C}}$ so that in optimal case $\boldsymbol{E} = \boldsymbol{E}^{\text{G}}$. In terms of spherical harmonic modes, the equation can be written as

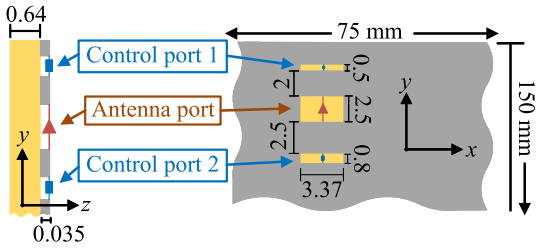

Fig. 2. Region of the test device where the antenna and the control ports are located. The gray color corresponds to the metallization and yellow to the substrate below the copper.

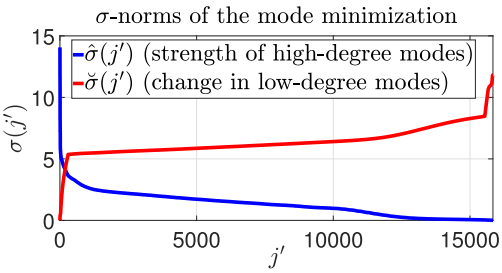

Fig. 3. σ-norms of the mode minimization as a function of the limit mode.

$\mathbf{Q}\boldsymbol{a} = \boldsymbol{q}^{\mathrm{G}}$, which leads us to the following formulation:

$$\begin{bmatrix} \check{\mathbf{Q}}^{\mathrm{C}} \\ \hat{\mathbf{Q}}^{\mathrm{C}} \end{bmatrix} \boldsymbol{a}^{\mathrm{C}} = \begin{bmatrix} \check{\boldsymbol{q}}^{\mathrm{G}} - \check{\mathbf{Q}}^{\mathrm{A}}\boldsymbol{a}^{\mathrm{A}} \\ -\hat{\mathbf{Q}}^{\mathrm{A}}\boldsymbol{a}^{\mathrm{A}} \end{bmatrix}. \tag{10}$$

The prior goal is to minimize the high-degree modes. Thus, we aim at finding $\boldsymbol{a}^{\mathrm{C}}$ that minimizes the norm $\hat{\sigma}(j') = ||\hat{\mathbf{Q}}^{\mathrm{C}}\boldsymbol{a}^{\mathrm{C}} + \hat{\mathbf{Q}}^{\mathrm{A}}\boldsymbol{a}^{\mathrm{A}}||$, where j' is the limit between low- and high-degree modes. This can be solved for instance, using the least-squares method. We have used the commonly used 2-norm, although some other norms might be useful as well.

The vector $\check{\boldsymbol{q}}^{\mathrm{G}}$ represents the low-degree modes of the target field. In addition to minimizing the high-degree modes, we strive to not to change low-degree modes in order to keep the general shape of the radiation pattern similar to the original pattern. Thus, we also analyze a norm $\check{\sigma}(j') = ||\check{\mathbf{Q}}^{\mathrm{C}}\boldsymbol{a}^{\mathrm{C}}||$, which has been induced from (10) by setting $\check{\boldsymbol{q}}^{\mathrm{G}} = \check{\mathbf{Q}}^{\mathrm{A}}\boldsymbol{a}^{\mathrm{A}}$. When calculating the weights for the control ports, j' is chosen such that both $\hat{\sigma}(j')$ and $\check{\sigma}(j')$ are as small as possible, but prioritizing to minimize $\hat{\sigma}(j')$.

III. Illustrative Example

A. Active Implementation

We demonstrate the method with structure in Fig. 2. The antenna is a grounded dielectric slab fed by a slot of size 3.37 × 2.50 mm. The structure models the display of a mobile phone. The substrate is 0.64-mm thick Rogers Ro3010 with $\epsilon_r = 10.2$ and $\tan\delta = 0.0022$. The size of the ground plane is 150 × 75 mm. The distance between the slot and the shorter edge of the device is 4 mm. The slot is located in the center of the shorter side of the device. The control ports are implemented as slots and placed close to the antenna feeding slot. They aim to minimize the vertical surface waves propagating to $-y$-direction. The horizontal surface waves could be minimized by placing control ports to $\pm x$ direction from the antenna slot. The simulated far fields radiated by each port are imported into MATLAB, and the control port feeding weights are calculated using the proposed method.

Relations between j'-values and σ-norms have been visualized in Fig. 3. As mentioned, the limit mode j' should be chosen so that both norms $\hat{\sigma}(j')$ and $\check{\sigma}(j')$ are small. However, since $\hat{\sigma}(j')$ decreases and $\check{\sigma}(j')$ increases monotonically with j', and these two quantities are not directly related to each other, j' cannot be chosen by analyzing only these quantities.

Even if the σ-measures do not describe explicitly, which j' value is optimal, they convey well the sensitivity of the results as a function of the domain of j'. At the center of the spectrum, the σ-norms do not change much as j' varies, unlike with small or large j'.

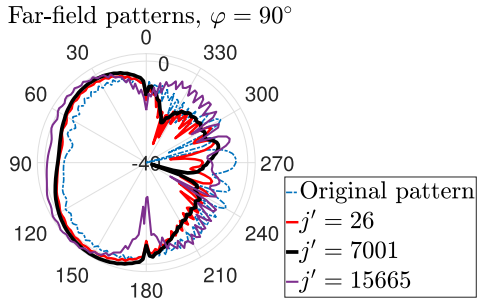

Fig. 4. Electric far fields in the yz plane, when modes higher than j' have been minimized with active control ports.

We apply the method using $j' = 26$, $j' = 7001$, and $j' = 15665$. The total number of modes in this antenna is $J = 15\,840$. Fig. 4 shows the far-field patterns after the mode minimization process with three different limit modes. Also the pattern where the control ports are not fed is visualized. The ripples in the radiation pattern seem to decrease most clearly with $j' = 7001$ but also significantly with $j' = 26$.

Based on our experience, if j' is at the center of the spectrum, the results are not very sensitive to the choice of the exact value of j', as can be deducted also from Fig. 3. The results obtained by setting $6000 < j' < 8000$ have no significant difference. We implement the active surface-wave minimization with $j' = 7001$.

Without cancellation, the radiation efficiency of the device is 97.13% and gain 5.98 dBi. With actively injected canceling waves and $j' = 7001$, the control port feeds are $a_2 = 0.24\angle -100°$ and $a_3 = 0.65\angle 64°$. The resulting radiation efficiency is 97.76% and the gain 6.78 dBi. When we minimize the surface waves, also the propagation losses of the surface waves suppress, which explains the almost unchanged efficiency. In this case, the active cancellation coefficients are reasonably low. If the coefficients were significantly strong, the control ports should be relocated or redesigned.

B. Passive Implementation

Launching the canceling surface waves is also possible with passive, fixed implementation. In order to do that, we study the system in Fig. 5. The antenna feeding ports are to the left of the n-port and the control ports to the right. The aim is to calculate the impedance loads $Z_p = R_p + jX_p$ for the control

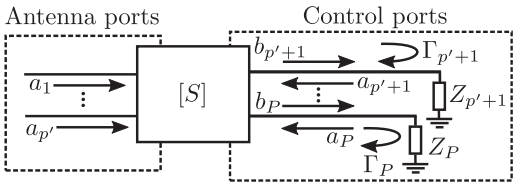

Fig. 5. Illustration of the incident and scattered waves at the ports of the device.

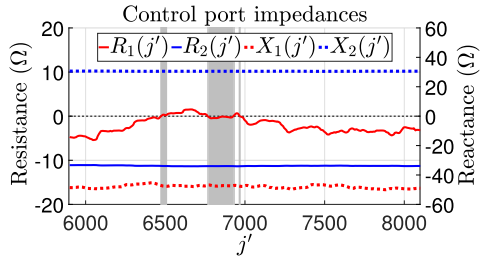

Fig. 6. Required impedance loads for control ports in order to minimize modes larger than j'.

ports $p \in [p'+1, P]$ such that the incident waves a_p are equal to the elements of $\boldsymbol{a}^{\mathrm{C}}$ solved from (10).

As described in [11], the required reflection coefficients Γ_p for the passive control ports can be solved as

$$\Gamma_p = \frac{a_p}{\sum_{i=1}^{P} S_{pi} a_i} \tag{11}$$

where the antenna is described with scattering parameters S_{ij}. Then, the impedance terminations for the control ports can be calculated as

$$Z_p = Z_0 \frac{1+\Gamma_p}{1-\Gamma_p} \tag{12}$$

where $Z_0 = 50\ \Omega$ is the reference impedance.

Implementing cancellation, either actively or passively, typically affects the impedance of the antenna port. Therefore, a matching circuit has been added to the antenna feeding port after implementing the control ports.

The obtained impedance values might have negative real parts. In practice, this indicates that the control ports should inject energy to the system, not only scatter it. In the optimal situation, the chosen j' gives a purely reactive Z_p for each control port. Then, the resistive components and active signals can be omitted from the control ports.

Fig. 6 illustrates the required control port impedances with values $6000 < j < 8000$ as the σ-norm analysis suggested. The curves also indicate if the successful cancellation is possible with the studied control port locations and topologies. The resistance of control port 1 is very close to zero when $j' \in \{[6470, 6510]; [6770, 6930]; 6967\}$. These domains are highlighted in gray in Fig. 6. By analyzing Z_2 on this domain, we see that its real part is negative. j' cannot be chosen so that $\Re\{Z_2\} = 0$, but since the resistance of control port 2 is still relatively low, we assume that it has only a minor effect on the results and can be, therefore, neglected.

For the passive implementation, we use value $j' = 6967$. The obtained components that would be inserted into the control ports are $C = 0.13$ pF for control port 1 and $L = 0.19$ nH for

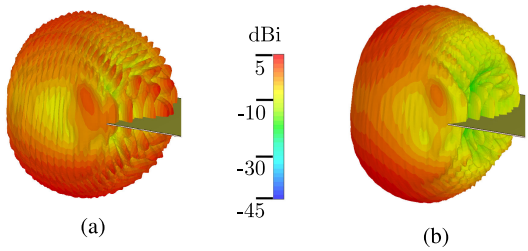

Fig. 7. Realized gain patterns. (a) No control ports. (b) Passive control ports with $j' = 6967$.

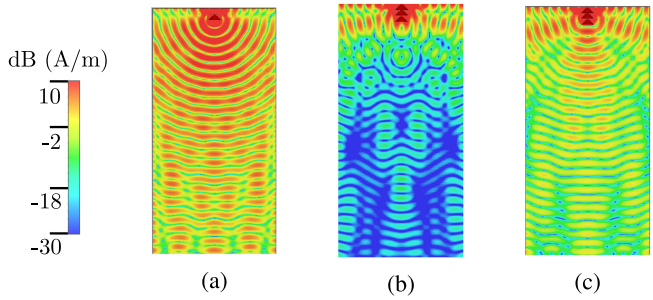

Fig. 8. Surface currents on the substrate face. (a) No canceling. (b) Active implementation with $j' = 7001$. (c) Passive implementation.

control port 2. Fig. 7 illustrates the radiation patterns before and after the surface-wave minimization with passive control ports. The ripply back lobes decrease significantly also when implementing the method with passive control ports, although the implementation does not fully correspond to the optimal feeds due to the negative real part being ignored.

Fig. 8 illustrates the surface currents. The figure compares the original currents, the currents obtained using active control ports, and the ones resulting from passively implemented surface-wave minimization. The surface waves are not suppressed as significantly as with the active control ports due to the neglected resistance of control port 2. Still, the surface waves are significantly weaker compared to the original case. The resulting radiation efficiency is 97.69% and gain 6.89 dBi. That is, the gain increases by 0.91 dBi.

IV. Conclusion

In this letter, we have demonstrated that the surface waves can be minimized using relatively small-sized additional structures. The design is systematic, computationally efficient, and does not require in-depth analysis of the surface waves. Both active and passive implementations are possible, resulting in significant improvement of radiation patterns and reduction of surface waves in both cases. Due to variations in surrounding environment, such as human body effect, active implementation with dynamically controlled cancellation signals might be useful in practice. The introduced method gives a general framework for surface wave minimization and offers a solid ground for further, more application-specific experiments on surface wave cancellation. As well, verifying the benefits of the method by antenna measurements could be considered in future.

REFERENCES

[1] R. Valkonen, A. Lehtovuori, and D. Manteuffel, "Capacitive coupling elements—Changing the way of designing antennas," in *Proc. 8th Eur. Conf. Antennas Propag.*, 2014, pp. 229–233.

[2] P. Vainikainen, J. Ollikainen, O. Kivekas, and K. Kelander, "Resonator-based analysis of the combination of mobile handset antenna and chassis," *IEEE Trans. Antennas Propag.*, vol. 50, no. 10, pp. 1433–1444, Oct. 2002.

[3] B. Xu, K. Zhao, Z. Ying, S. He, and J. Hu, "Investigation of surface waves suppression on 5G handset devices at 15 GHz," in *Proc. 10th Eur. Conf. Antennas Propag.*, 2016, pp. 1–4.

[4] Z. Yang, J. Xiao, and Q. Ye, "Enhancing MIMO antenna isolation characteristic by manipulating the propagation of surface wave," *IEEE Access*, vol. 8, pp. 115572–115581, 2020.

[5] F. Yang and Y. Rahmat-Samii, "Microstrip antennas integrated with electromagnetic band-gap (EBG) structures: A low mutual coupling design for array applications," *IEEE Trans. Antennas Propag.*, vol. 51, no. 10, pp. 2936–2946, Oct. 2003.

[6] V. R. Komanduri, D. R. Jackson, J. T. Williams, and A. R. Mehrotra, "A general method for designing reduced surface wave microstrip antennas," *IEEE Trans. Antennas Propag.*, vol. 61, no. 6, pp. 2887–2894, Jun. 2013.

[7] S. Mahmoud and A. R. Al-Ajmi, "A novel microstrip patch antenna with reduced surface wave excitation," *Prog. Electromagn. Res.*, vol. 86, pp. 71–86, 2008.

[8] R. Rodríguez-Cano, S. Zhang, and G. F. Pedersen, "Transparent mm-wave array on a glass substrate with surface wave reduction," in *Proc. 14th Eur. Conf. Antennas Propag.*, 2020, pp. 1–4.

[9] B. Boesman, D. Pissoort, G. Gielen, and G. Vandenbosch, "Fast and efficient near-field to near-field and near-field to far-field transformation based on the spherical wave expansion," in *Proc. IEEE Int. Symp. Electromagn. Compat.*, 2015, pp. 529–534.

[10] A. S. Kaddour, A. Clemente, S. Bories, and C. Delaveaud, "Design of high directivity compact parasitic array for beam-steering applications," in *Proc. 9th Eur. Conf. Antennas Propag.*, 2015, pp. 1–5.

[11] A. Clemente, M. Pigeon, L. Rudant, and C. Delaveaud, "Design of a super directive four-element compact antenna array using spherical wave expansion," *IEEE Trans. Antennas Propag.*, vol. 63, no. 11, pp. 4715–4722, Nov. 2015.

[12] J. E. Hansen, Ed., *Spherical Near-Field Antenna Measurements* (Electromagnetic Waves). Stevenage, U.K.: Peregrunus, 1988.

[13] B. Fuchs, L. Le Coq, S. Rondineau, and M. D. Migliore, "Fast antenna far-field characterization via sparse spherical harmonic expansion," *IEEE Trans. Antennas Propag.*, vol. 65, no. 10, pp. 5503–5510, Oct. 2017.